Annals of Biomedical Engineering, Vol. 30, pp. 808–827, 2002
Printed in the USA. All rights reserved.

0090-6964/2002/30(6)/808/20/$15.00

A Computational Model for Glycogenolysis in Skeletal Muscle

MELISSA J. LAMBETH[1] and MARTIN J. KUSHMERICK[1,2,3]

[1]Department of Bioengineering, [2]Department of Radiology, and [3]Department of Physiology and Biophysics, University of Washington, Seattle, WA

(Received 23 August 2001; accepted 10 May 2002)

Abstract—A dynamic model of the glycogenolytic pathway to lactate in skeletal muscle was constructed with mammalian kinetic parameters obtained from the literature. Energetic buffers relevant to muscle were included. The model design features stoichiometric constraints, mass balance, and fully reversible thermodynamics as defined by the Haldane relation. We employed a novel method of validating the thermodynamics of the model by allowing the closed system to come to equilibrium; the combined mass action ratio of the pathway equaled the product of the individual enzymes' equilibrium constants. Adding features physiologically relevant to muscle—a fixed glycogen concentration, efflux of lactate, and coupling to an ATPase—allowed for a steady-state flux far from equilibrium. The main result of our analysis is that coupling of the glycogenolytic network to the ATPase transformed the entire complex into an ATPase driven system. This steady-state system was most sensitive to the external ATPase activity and not to internal pathway mechanisms. The control distribution among the internal pathway enzymes—although small compared to control by ATPase—depended on the flux level and fraction of glycogen phosphorylase a. This model of muscle glycogenolysis thus has unique features compared to models developed for other cell types. © *2002 Biomedical Engineering Society.* [DOI: 10.1114/1.1492813]

Keywords—Metabolism, Flux analysis, Enzyme kinetics.

INTRODUCTION

Glycolysis was the first metabolic pathway to develop in evolution. It is centrally important to intermediary metabolism in all cells. The kinetic mechanisms of its component enzymes in many cell types have been well characterized. Glycolysis has fascinating nonlinear and oscillatory properties of feedback inhibition that warrant quantitative description. Much of the modeling effort has been focused on erythrocytes,[29,39] yeast,[61] and T. brucei.[3] One common result from all of this work seems to be that regulation of flux in this pathway occurs by separate mechanisms in the different cell types. It may be a general principle that regulation of flux in the pathway depends more on cell properties and reactions extrinsic to the pathway itself than on the basic properties of the enzymes in the pathway. The work presented here is motivated by questions and issues relevant both to modeling of metabolic networks *per se* as well as to understanding the role of glycogenolysis and glycolytic fluxes in muscle energy metabolism.

Modeling of glycolysis in muscle has not been extended since initial efforts by Garfinkel *et al.* in 1968,[22] for a number of possible reasons: (1) the large dynamic range of fluxes [$\sim$0.6–60 mM ATP/min (Ref. 12)]; (2) large changes in metabolite concentrations (lactate, inorganic phosphate, and phosphocreatine) due to muscle properties and intensity and duration of activity; (3) uncertainty in the kinetic function and substrate concentration describing the glycogen phosphorylase reaction; and (4) lack of consensus regarding the control mechanisms that regulate flux.[10,12,15]

Our approach is to develop a parsimonious model of glycogenolysis to enable future tests of conflicting hypotheses concerning controls of its flux in particular muscle types and to investigate how glycogenolytic and glycolytic fluxes are regulated when connected to other key reactions in muscle energy balance, such as the creatine and adenylate kinases and ATPases. We developed this model of muscle glycogenolysis to address three questions:

(1) Is there a value in making all the reactions biochemically reversible in the equations? We explore the consequences of the use of irreversible reaction steps in metabolic modeling. Equation simplification by irreversibility limits the possible steady states allowed in the system. More importantly, it is incorrect in principle due to microscopic reversibility.[13] We explored a reaction scheme in which all component reaction steps were fully reversible (despite the fact that some have a very favorable unidirectional thermodynamic driving force). We will show that a detailed mathematical analysis of a reversible scheme proves to be valuable because it allows the use of thermodynamics as a tool to validate the model.

(2) What are the consequences of coupling glycogenolysis to other reactions within the cell on the regulation of its pathway flux? The stoichiometry and conserved moieties of the pathway and its functional relations with other intracellular processes, e.g., ATPases,

creatine and adenylate kinases, and mitochondrial oxidative phosphorylation, provide constraints in modeling by reducing the overall degrees of freedom. The degree of complexity may be reduced by addition of stoichiometrically coupled reactions to the main pathway. When the rates of the ATPase reaction and ATP synthesis are rapid, creatine kinase and adenylate kinase are necessary for effective buffering of the ATP/ADP/AMP ratios. The consequence of this buffering is that different ATPase activities change the ATP/ADP/AMP ratio relatively little as compared to the large increase in P_i. Thus, depending on cell type, the presence of these buffers will affect differently the flux and metabolite distribution within glycolysis. These results may lead to a general principle that models of particular networks, even if the kinetic parameters in the model are similar, will have different behaviors and possibly different overall regulations depending on the environment in which the network of glycolytic and glycogenolytic reactions operates.

(3) What aspects of the network of reactions are able to account for the ability to achieve and sustain a wide range of fluxes? Muscle activity is able to change the relevant metabolic fluxes over a large range, up to 100-fold depending on the intensity and type of activity.[12] Existing models in other cell types do not attempt to account for a significant dynamic range, nor do the models account for a wide range of steady states observed experimentally in muscles.[29,39,61] We coupled ATPase flux with glycolytic and glycogenolytic fluxes. We find this coupling produces additional stoichiometric constraints, which have the effect of simplifying the total system.

METHODS

Development of the Model

The abundant information on glycogenolytic enzyme kinetics in the literature was compiled into a consensus list of substrate and product concentrations and kinetic parameters for each enzyme (Tables 1, 2, and 3). The model consisted of the rate equations for 12 reactions from glycogen to lactate in skeletal muscle (Fig. 1). The basic glycogenolytic model describes the complete pathway from glycogen to lactate plus the inclusion of adenylate kinase and creatine kinase. To this basic model (which is a closed system of the glycolytic network), we added additional reactions important for muscle energetics and determined the components necessary for the model to reach steady state in both a closed and in an open system.

The glycolytic pathway, represented by this model, is purposely considered to be an isolated pathway that does not interact with other metabolites, reactions, or pathways. The behavior of this model, therefore, reflects how the glycogenolytic system will behave without extrinsic signaling, without free transport of monocarboxylates by the blood supply, without glucose uptake and phosphorylation via hexokinase, and without additional redox reactions such as glycerol-3-phosphate dehydrogenase and mitochondrial oxidative phosphorylation. The primary reason for these choices is to characterize the pathway itself as a functional unit.

Several features in the description of the pathway are different from existing glycolytic models available for other cellular systems. Inorganic phosphate is described as a variable in the model due to its dramatic range of concentrations (2–30 mM) in skeletal muscle.[11] NAD/NADH is also allowed to vary, consistent with the chosen absence of interaction with other cellular systems.

The glycolytic model is a continuum model that is based on standard differential equation form, with the derivatives of the metabolite concentrations (fluxes) formulated by the velocity expressions for the enzymes (see the Appendix). Descriptions of the fluxes are in Michaelis–Menten form with substrate–product, allosteric, or rapid equilibrium bi–bi kinetics. The decisions on the type of kinetic equation used were based on known behavior of the enzyme *in vitro* and on available parameter values in the literature; values and functions used in the model are given in Table 1 and in the Appendix. Ordered Michaelis–Menten kinetics were used as a default form in bi–bi reactions, when altered affinity binding constants could not be determined from the literature, as defined by Eq. (1):

$$V = \frac{\dfrac{V_{\max f} AB}{K_a K_b} - \dfrac{V_{\max r} PQ}{K_p K_q}}{1 + \dfrac{A}{K_a} + \dfrac{B}{K_b} + \dfrac{AB}{K_a K_b} + \dfrac{P}{K_p} + \dfrac{Q}{K_q} + \dfrac{PQ}{K_p K_q}}. \quad (1)$$

It differs from a Cleland, or random bi–bi reaction, by the absence of an altered affinity for the second substrate (or product in the reverse direction) after the first substrate is bound, effectively resulting in an ordered bi–bi rapid equilibrium reaction as defined by Segel.[56]

In order to determine whether rapid-equilibrium assumptions are suitable for dynamic metabolic modeling, we included the full reversible enzyme kinetic equation for all enzyme reactions in the pathway. Kinetic controls via the near-equilibrium enzymes are often omitted from models of glycolysis, especially phosphoglucomutase and enolase, but we will show these reactions have important influences on the dynamic behavior. The reverse direction $V_{\max}$ values were calculated using the Haldane expression (see below in the section on thermodynamic constraints).

We define, for the purposes of this paper, the redox potential, NAD/NADH, as $\sim R$ (note this is the inverse of the common nomenclature in the mitochondria) and

TABLE 1. Model kinetic parameters.

Enzyme	Parameter	Literature values (mM unless noted)	Species	Reference	Model value (mM unless noted)
Glycogen Phosphorylase *A*	K_{eq}	0.42 (unitless)		28	0.42 (unitless)
	K_{GLYf}	1.7	Rabbit	23	1.7
	K_{P_i}	4		23	4
	K_{iGLY}	2		23	2
	K_{iP_i}	4.7		23	4.7
	K_{GLYb}	0.15		23	0.15
	K_{G1P}	2.7		23	2.7
	K_{iG1P}	10.1		23	10.1
Glycogen Phosphorylase *B*	K_{eq}	0.42 (unitless)		28	0.42 (unitless)
	K_{P_i}	0.2	Rabbit	19	0.2
	K_{ip_i}	4.6		19	4.6
	K_{iGLYf}	15		19	15
	K_{G1P}	1.5		19	1.5
	K_{iG1P}	7.4		19	7.4
	K_{iGLYb}	4.4		19	4.4
	K'_{AMP}	1.9e-6	Rabbit	14	1.9e-6
	nH	1.75		14	1.75
Phosphoglucomutase	K_{eq}	16.62 (unitless)		28	16.62 (unitless)
	K_{G1P}	0.063	Rabbit	30	0.063
	K_{G6P}	0.03		30	0.03
Phosphoglucoisomerase	K_{eq}	0.45 (unitless)		28	0.45 (unitless)
	K_{G6P}	0.48	Mouse	49	0.48
	K_{F6P}	0.031	Rabbit	31	0.119
Phosphofructokinase	K_{eq}	242 (unitless)		28	242 (unitless)
	K_{F6P}	0.18	Rabbit	40	0.18
	K'_{F6P}	20		40	20
	K_{ATP}	0.08		40	0.08
	K'_{ATP}	0.25		40	0.25
	K_{FBP}	4.02	Rabbit	36	4.02

TABLE 1. (Continued).

	K'_{FBP}	⋯			4.02
	K_{ADP}	2.71		36	2.7
	K'_{ADP}	⋯			2.7
	K_{iATP}	0.87		40	0.87
	K_{aAMP}	⋯			0.06
	d	0.01 (unitless)		40	0.01 (unitless)
	e	⋯			0.01 (unitless)
	L_o	13 (unitless)		40	13 (unitless)
Aldolase	K_{eq}	9.5e-5 (M^{-1})		28	9.5e-5 (M^{-1})
	K_{FBP}	0.05			0.05
	K_{DHAP}	2.1	Rabbit	45	2
	K_{GAP}	1.1		45	1
Triose Phosphate Isomerase	K_{eq}	0.052 (unitless)		28	0.052 (unitless)
	K_{GAP}	0.32	Rabbit	34	0.32
	K_{DHAP}	0.61	Human	16	0.61
Glyceraldehyde-3-Phosphate Dehydrogenase	K_{eq}	0.089 (unitless)		28	0.089 (unitless)
	K_{GAP}	0.0025		63	0.0025
	K_{NAD}	0.09		63	0.09
	K_{P_i}	0.29	Rabbit	21	0.29
	K_{13BPG}	0.0008		63	0.0008
	K_{NADH}	0.0033		63	0.0033
Phosphoglycerate Kinase	K_{eq}	57,109 (unitless)		28	57109 (unitless)
	K_{13BPG}	0.0022	Rabbit	33	0.002
	K_{ADP}	0.05	Pig	38	0.008
	K_{3PG}	1.2		33	1.2
	K_{ATP}	0.36	Rabbit	20	0.35
Phosphoglycerate Mutase	K_{eq}	0.18 (unitless)		28	0.18 (unitless)
	K_{3PG}	0.2	Chicken	52	0.2
	K_{2PG}	0.014		52	0.014
Enolase	K_{eq}	0.49 (unitless)		28	0.49 (unitless)
	K_{2PG}	0.12	Rat	51	0.1
	K_{PEP}	0.37		51	0.37

TABLE 1. (Continued).

Pyruvate Kinase	K_{eq}	10304 (unitless)		28	10304 (unitless)
	K_{PEP}	0.08	Rat	27	0.08
	K_{ADP}	0.3		27	0.3
	K_{PYR}	7.05	Rabbit	18	7.05
	K_{ATP}	0.82–1.13		18	1.13
Lactate Dehydrogenase	K_{eq}	16,198 (unitless)		28	16198 (unitless)
	K_{PYR}	0.6	Pig	5	0.335
	K_{NADH}	0.008		57	0.002
	K_{LAC}	17	Mouse	41	17
	K_{NAD}	0.253	Rabbit	66	0.849
Creatine Kinase	K_{eq}	233 (unitless)	Rabbit	54	233 (unitless)
	K_{PCr}	1.11		54	1.11
	K_{iATP}	3.5		54	3.5
	K_{iADP}	0.135		54	0.135
	K_{iPCr}	3.9		54	3.9
	K_{Cr}	3.8		54	3.8
Adenylate Kinase	K_{eq}	2.21 (unitless)	Rabbit	17	2.21 (unitless)
	K_{AMP}	0.32	Human	62	0.32
	K_{ATP}	0.27		62	0.27
	K_{ADP}	0.35		62	0.35

TABLE 2. Enzyme activities.[a]

Enzyme	Activity (U/mg)	Conc. (mg/ml)	Species	V_{max} (M/min)
GPP *B*	25	0.6×2	Rabbit	0.03
GPP *A*	25	0.4×2	Rabbit	0.02
PGLM	800	0.6	Pig	0.48
PGI	1100	0.8	Pig	0.88
PFK	160	0.35	Rabbit	0.056
ALD	16	6.5	Rabbit	0.104
TPI	6000	2	Rabbit	12.0
GAPDH	115	11	Rabbit	1.265
PGK	800	1.4	Pig	1.12
PGM	1400	0.8	Rabbit	1.12
EN	80	2.4	Rabbit	0.192
PK	450	3.2	Rabbit	1.44
LDH	600	3.2	Pig	1.92
ADK	2200	0.4	Pig	0.88
CK	100	5	Pig	0.5

[a]See Ref. 55.

the phosphorylation potential, $ATP/(ADP \cdot P_i)$, as $\sim P$. We chose this definition of energetic driving force for our purposes (instead of using a stoichiometric relation, e.g., Atkinson's energy charge) due to the availability of inorganic phosphate measurements, the need to include P_i due to its large changes, and the undersaturation of adenylate kinase by AMP at all physiological concentrations in skeletal muscle.

Simplification of the Model

The model contains no external effectors; any inhibitors or activators in the equations are metabolites variable elsewhere in the model. For this reason, citrate, fructose-2,6-diphosphate and calcium ion are not present in the equations. An additional simplification is the assumption that all cationic-bound species have the same affinity for the enzyme and can be described generically

TABLE 3. Averaged resting concentrations used for initial conditions.[a,b]

Metabolite	Concentration (mM)
GLY	112
G1P	0.0589
G6P	0.75
F6P	0.228
FBP	0.0723
DHAP	0.0764
GAP	0.0355
13BPG	0.065*
3PG	0.052
2PG	0.005*
PEP	0.0194
PYR	0.0994
LAC	1.3
ATP	8.2
ADP	0.013
AMP	2e-5
P_i	4.1
PCr	34.67
NAD	0.5

[a]See Refs. 2, 8, 24, and 53.
[b]Concentration unreported for skeletal muscle. Estimated values are based upon orders of magnitude seen in other cell types.

in one pool as ΣATP, ΣADP, ΣAMP, ΣP_i, etc. The model thus exists implicitly at constant pH, fixed concentration of Mg^{++} and other ions.

Table 1 lists the *in vitro* literature values for each parameter describing the kinetics of the model reactions, as well as the precise values we used for our calculations. Values from sources—at physiological pH (7.0) and temperature (37 °C) when available—of mammalian skeletal muscle origin were utilized. In addition, if information could be obtained all from the same source, we chose to use those values, as they would be more consistent relative to one another. V_{max} values were calculated in M/min (molar concentration in cellular water per minute) from the known specific activity of the enzyme in U/mg multiplied by the approximate concentration of the enzyme in the cell by mg/ml, as shown in Table 2. We obtained the values for the enzyme concentrations and activities from Scopes *et al.*,[55] measured in skeletal muscle extracts and in purified enzymes from the same source. The reverse direction V_{max} values were calculated by the Haldane expression. Initial concentrations of the variable metabolites have been defined by averaging three sources of biopsy data from rat and human resting skeletal muscle (Table 3); 13BPG and 2PG were estimated by the order of magnitude reported for other cell types.

Constraints by Mass Conservation

Constraints on the system are in the form of mass relations and the assumptions cited above. The total

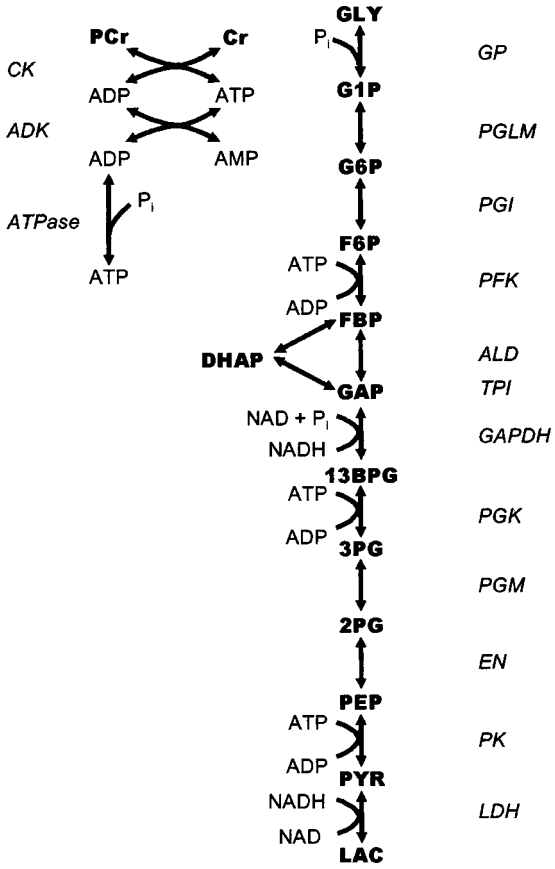

FIGURE 1. Schematic representation of all reactions used in the model.

adenosine nucleotides is a fixed number such that 8.2 mM ATP + 0.0013 mM ATP + 1e-5 mM AMP = 8.21301 mM; this quantity is consistent with measured values of human skeletal muscle ATP content in intracellular water.[11,24] Likewise, phosphocreatine and creatine are constrained to sum to 40 mM.[24,44] 0.5 μM NADH + 0.5 mM NAD equals a fixed amount of 0.5005 mM (with a starting $\sim R$ ratio of 1000).[37,53] These are the simplest of the constraints by conserved moieties.

Correct conservation of mass within the model was proven for both open and closed systems by calculating the total phosphate using the following equation:

$$\Sigma P = G1P + G6P + F6P + (2\text{FDP}) + \text{DHAP} + \text{GAP} + (2 \times 1,3\text{BPG}) + 3PG + 2PG + PEP + (2\text{ATP}) + \text{ADP} + \text{PCr} + P_i . \quad (2)$$

The number of sites available for phosphate transfer determines the stoichiometry in Eq. (2). Thus, AMP is not included in this definition of total phosphate but it would be added for a tally of soluble phosphate content of metabolites. The structure of the model results in a con-

stant sum of all substrates and products for the closed system. The open system is defined via an ATPase term, which is coupled to the ADP, ATP, and P_i derivatives; the sum of the concentrations in Eq. (2) also remains constant with a steady-state flux through the pathway (see the Results).

In the same manner, the total mass of oxidized and reduced intermediates must be maintained by the moiety:

$$\text{total oxidized} = \text{NAD} + \text{1,3BPG} + \text{3PG} + \text{2PG} + \text{PEP} + \text{PYR},$$

$$\text{total reduced} = \text{NADH} + \text{GAP} + \text{LAC}. \quad (3)$$

Thermodynamic Constraints

The reverse $V_{\max}$ parameter values are calculated based upon the Haldane relation:

$$V_{\max\ \text{reverse}} = \frac{V_{\max\ \text{forward}} K_{m\text{reverse}}}{K_{m\text{forward}} K_{\text{eq}}}. \quad (4)$$

Because all equations are reversible when defined in this manner the metabolites can be allowed to equilibrate in the closed system to test the validity of the model thermodynamically. By constructing the model with built-in Haldane relations, no adjustment/optimization of the parameters will violate the thermodynamics of any reaction or of the entire network.

The combined equilibrium constant is calculated by using the total products over reactants, assuming that $\text{glycogen}_{n-1}/\text{glycogen}_n$ is unity. By multiplying each reaction's product/reactant ratio (Γ) together, all intermediates cancel out except for the expression in Eq. (5):

$$K_{\text{eqcombo}} \equiv \text{LAC}^2 \left(\frac{\text{ATP}}{\text{ADP}P_i} \right)^3. \quad (5)$$

For conditions other than the standard state, the product of the terms (ΓK_{eqobs}) for each reaction (i), equals K_{eqcombo}:

$$K_{\text{eqcombo}} = \prod_{i=1}^{12} K^m_{\text{eq}_{i\ \text{thermo}}} = \prod_{i=1}^{12} (\Gamma K^m_{\text{eq}_{i\ \text{obs}}}),$$

where

$$m = \begin{cases} 1, & \text{GP} \rightarrow \text{ALD} \\ 2, & \text{GAPDH} \rightarrow \text{LDH}. \end{cases} \quad (6)$$

Power m accounts for the branching of the six-carbon intermediates into two three-carbon intermediates at aldolase. Note that the directionality of triose-phosphate isomerase towards the production of glyceraldehyde 3-phosphate is used in Eqs. (5) and (6).

Numerical Integration

The model was constructed of algebraic and differential equations using the SAAMII (SAAM Institute, Seattle, WA) software program and numerically integrated using a Rosenbrock semi-implicit method with a relative error of 0.000 01 and an absolute error of 0.000 001. The numerical results were identical when checked by integration with GEPASI (http://www.gepasi.org/). Subsequent sensitivity analysis was performed by translating the model into XSIM (National Simulation Resource, Seattle, WA) and numerically integrated using an implicit Runga–Kutta method of variable order (RADAU) with an error of less than 0.001%.

RESULTS

Thermodynamic Validation

The model used for this analysis is as depicted in Fig. 1, without an ATPase; without ATPase the network is a closed system. This closed system of 12 enzymes does produce a steady state, the one at equilibrium where the forward and reverse fluxes are equal and net flux asymptotes to zero. We take advantage of the drive towards equilibrium to give a method of validation for our model. Because the Haldane relation has described each reaction reversibly, the mass action ratios (products/reactants of each reaction) of the closed system's stationary state should come to equilibrium. The distribution of mass should be defined as the product of the individual equilibrium constants.

We set the initial concentrations of the metabolites to standard conditions (1 M) prior to integration, as these are the conditions under which the equilibrium constants are measured. We integrated the model until a stationary state occurred (approximately 5000 min in simulation time). This condition defines the second term in Eq. (6), $\Pi_{i=1}^{12} K^m_{\text{eq}_{i\ \text{thermo}}}$. We find that the model achieves numerical values consistent with the mass action ratios compared to the equilibrium constants applied to the model, upholding Eq. (6). The overall K_{eq} ($\Pi_{i=1}^{12} K^m_{\text{eq}_{i\ \text{thermo}}}$) has a value of 1.5572e19 as reported for glycogen→lactate (Johnson,[28] as tabulated in Mahler and Cordes[35]) while the model for standard state results in a $K_{\text{eqcombo}} = 1.5597\text{e}19$. The resulting values are indistinguishable within the accuracy of the experimental results for K_{eqthermo} (ΔG_o measured to two significant digits) and the numerical error of the integration. The compilation of the inputted K_{eqthermo} values is independent of the calculation, i.e., no adjustment or fitting of the model was

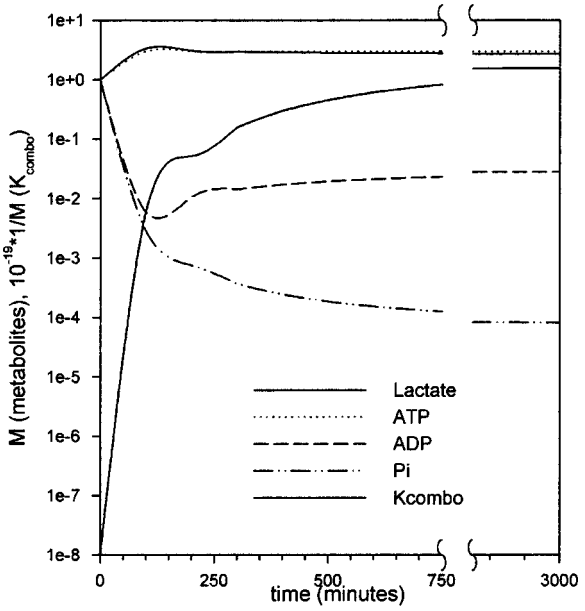

FIGURE 2. Approach of metabolites towards equilibrium. Initial conditions are standard (1 M) for all metabolites. $K_{eqcombo}$ (M^{-1}) is multiplied by 10^{-19} for visual purposes.

performed to achieve these results. Because of the relation expressed in Eq. (6), the mass in the system will be distributed with the same resulting product/substrate ratios regardless of initial conditions. This was achieved with our model using the physiological initial conditions from Table 3. This analysis validates the model and its parameters on the basis of their thermodynamic properties.

Figure 2 displays the time course for the approach to equilibrium of each contributor to the combined equilibrium constant of Eq. (5). The large decrease in inorganic phosphate, displayed as $1/(P_i^3)$ in Eq. (5), dominates the $K_{eqcombo}$ term, causing it to rise as it approaches equilibrium, while ATP and lactate remain at the same order of magnitude for the time course. The progress curves for the network of reactions were integrated by the model equations. These results show a depletion of the large stores of glycogen toward lactate until the inorganic phosphate, a cosubstrate in the glycogen phosphorylase reaction, reaches a concentration low enough that the entire system reaches equilibrium. Because P_i is also used at the GAPDH step, the decrease in its concentration results in (1) an increase of the triose phosphates, which in turn slows down PFK and aldolase; (2) a decrease in substrate (e.g., 1,3BPG) available for the kinases such that ATP cannot be synthesized; and (3) a lower NADH concentration that slows down the catalysis of pyruvate to lactate through LDH. The latter finding is exacerbated by pyruvate kinase, which has a greater difference between the observed free energy and the $\Delta G°$ than LDH. Thus, more mass builds up at pyruvate than lactate at equilibrium.

The results from this equilibrium analysis, while trivial on one level, provide an opportunity that should be of general interest for modeling. Naturally, the model should arrive at equilibrium because it is a closed system of fully reversible equations. The convergence of the mass to the theoretical mass action ratios is as expected due to the imposed Haldane relation on the reverse V_{max} parameter. But, in fact, these equalities (or lack thereof) also provide a useful and novel test of the validity of the equations.

Inorganic phosphate depletion through glycogen phosphorylase prevents the closed model from achieving a steady state except at equilibrium. This property makes it impossible to compute sensitivities. It also suggests that the analysis of glycolysis as an isolated system is fruitless, for it is only when features are added to the pathway to maintain the mass balance far from equilibrium that realistic behavior is simulated.

Forcing the Model to Steady State

One method of forcing the system into a steady state is to create a closed loop—an efflux of lactate from the system equal to $\frac{2}{3}$ ATPase and an influx into the system at glycogen of $\frac{1}{3}$ ATPase; the coefficients are determined by the stoichiometry of the system of reactions. Then, the rate of carbohydrate utilization is tightly regulated due to the forced addition and subtraction of mass from the pathway at the beginning and end. The problem with this approach is the inherent and fixed coupling of the flux to the ATPase; this was not analyzed further.

Instead, we found that specification of three conditions to the model was needed in order to achieve a physiologically realistic steady-state system—(1) holding the glycogen constant, (2) allowing an efflux from lactate into an infinite sink, and (3) adding an ATPase. The branched structure of glycogen, the localization of the phosphorylase enzyme within the glycogen particle, and the effective concentration of glucosyl moieties at about 100 mM justify the constant apparent glucosyl concentration at the enzyme. Next, we added an output from lactate that is dependent on the lactate concentration. By using a mass action coefficient (with an arbitrary value of 0.2), we are in effect simulating a flushing of a fraction of the lactate pool from the cytosol as would occur by the monocarboxylate transporter into the extracellular fluid and blood stream, but here in a nonsaturating, concentration-dependent manner. This condition is not meant to represent the physiological lactate efflux. The first two conditions, as illustrated by the lactate efflux in Fig. 3, are not sufficient by themselves for creating a steady-state system due to a continuous utilization of P_i with no reactions contributing to P_i production (except

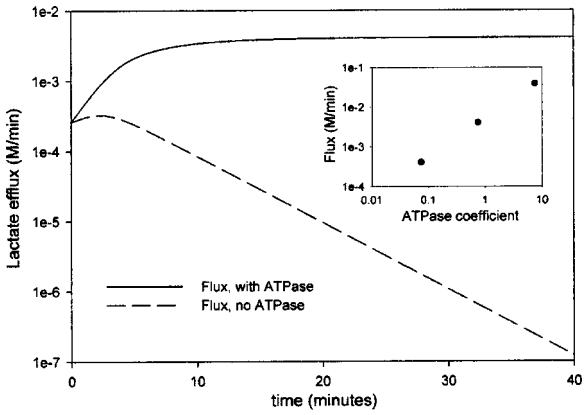

FIGURE 3. Demonstration of steady-state lactate efflux created with addition of the ATPase to the model. Inset: log–log plot of lactate flux vs ATPase coefficient.

for the small reversible flux of GP and GAPDH).

The essential requirement for the model to realize a steady-state flux is the addition of an ATPase. The ATP utilization is defined by a simple mass action flux, $V_{\mathrm{ATPase}} = k\mathrm{ATP}$, where k is a rate constant that can be assigned different values to represent various levels of ATP hydrolysis appropriate for graded muscle activity. Small values of k represent a muscle at rest and large values represent a muscle actively contracting at higher ATPase activity. The addition of an ATPase causes a balanced stoichiometry, and thus steady state; the ATPase must consume ATP at a rate three times faster than the breakdown of one glucosyl unit to lactate. With these constraints on the input to glycogen and efflux of lactate, steady states were achieved, but the flux through the system became a function of the ATPase flux, as we describe in the next two paragraphs and results in Table 4.

We chose to examine the system under different energetic requirements. We studied the system driven with graded ATPase flux values, approximately 0.6, 6, and 60 mM/min, to represent three energetic steady states of the muscle—resting, moderate exercise, and maximal exercise conditions (Table 4). The physiological appropriateness of the energetic steady states was based on the resultant orders of magnitude of the phosphorylation potential compared to published NMR data.[10,11] The ratio of phosphorylase $a:b$ was fixed across all three states as 40%:60 (a fraction of isozyme distribution observed during muscle activity[55]). Like a real physiological system, the flux through the system adjusts to the ATPase even though the input (fixed glycogen) and output (lactate efflux) are not directly coupled to the ATP sink. The ATPase reaction is coupled to the system by requirements of moiety conservation at the sites involving ATP, ADP, and P_i coupling.

TABLE 4. Values for the three physiological states. Rest corresponds to a fixed ATPase value of 0.6 mM/min, moderate exercise has an ATPase value of 6.1 mM/min, and maximal exercise has an ATPase rate of 58.4 mM/min. Refer to the text for more details.

Physiological State	Rest (mM)	Moderate exercise (mM)	Maximal exercise (mM)
ATPase coefficient	0.075	0.75	7.5
ATP flux (mM/min)	0.6	6.1	58.4
ATP	8.2	8.2	7.8
ADP	0.0078	0.032	0.415
AMP	3.3E-6	5.7E-5	0.010
P_i	0.64	7.1	31.5
PCr	32.8	28.6	3.0
NAD/NADH	513	12	1

This property is important for subsequent control analysis of the system. Although the network of glycogenolytic and glycolytic enzymes are poised far from equilibrium when coupled to the ATPase, a steady-state systemic flux can occur only with continuous ATP hydrolysis and synthesis. Table 4 shows the 1:1 relationship between the resultant systemic flux and each ATPase level in addition to the steady-state values of key metabolites. From the fact that steady-state concentrations are arrived at for the varied energetic demands that closely mimic observed values for skeletal muscles, we can assume that the assigned kinetic parameter values are appropriate for the model. Note that in the actual fluxes reported, the metabolite concentrations and enzyme activity used represent generic consensus values in the literature. Specific muscle cell types may vary in these properties and so will the characteristics of their specific fluxes and distributions of mass; these are matters for future analyses.

Sensitivity Analysis of the Model in Induced Steady State

For a sensitivity analysis of the model, each enzyme $V_{\max}$ and metabolite initial value in the model was perturbed by 1%. The sensitivity run calculated the sensitivity S_p^y of the variable (y) of interest to the parameter (p) being tested by the following equation:

$$S_p^y = \frac{\partial \ln y(p,t)}{\partial \ln p}. \tag{7}$$

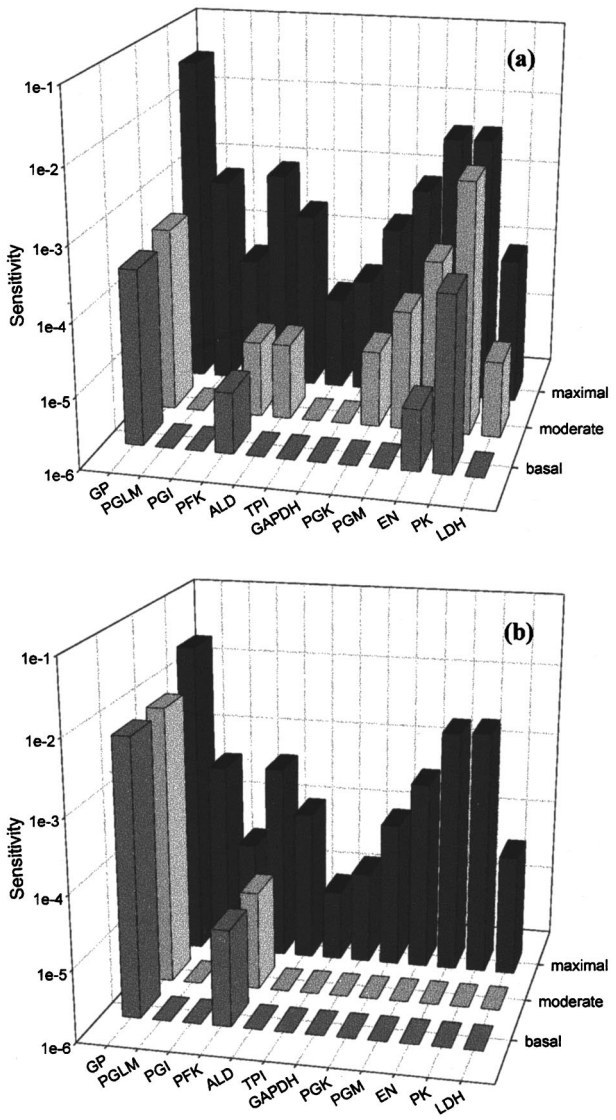

FIGURE 4. Flux control of pathway with efflux, ATPase, CK, and ADK omitted. Sensitivities were calculated based upon 1% perturbations of the V_{max} values for each reaction and the resultant change in steady-state systemic flux. (a) Phosphorylase *a* set at 40%; (b) phosphorylase *a* set at 1%. Zero values are plotted on the graphs as 1e-6 for illustrative purposes.

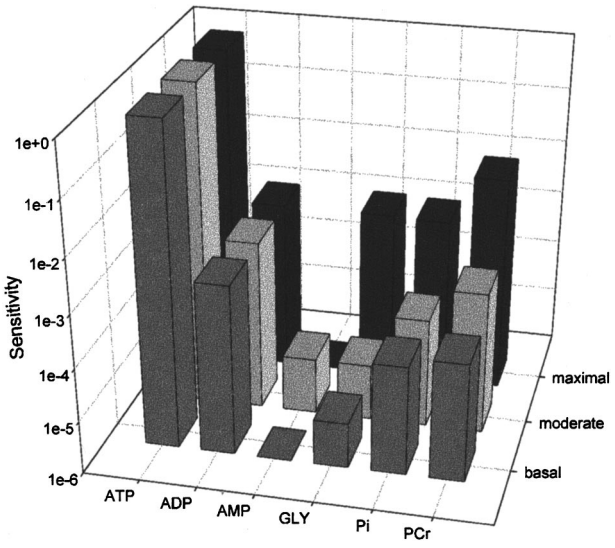

FIGURE 5. Flux sensitivity plot of initial conditions of key metabolites. Sensitivities were determined by perturbing starting concentrations by 1% and calculating the resulting change on the overall steady-state systemic flux. Glycogen is a parameter, not an initial condition in this plot. Zero values are plotted on the graph as 1e-6 for illustrative purposes.

For this sensitivity analysis, the function of interest $y(p,t)$ was either the steady-state metabolite concentration or steady-state flux as defined by the efflux from lactate. The parameter p being perturbed was an initial condition for one of the variable metabolites in the model or the V_{max} parameter of a given enzyme step. Equation (7) is equivalent to the response coefficient as defined by metabolic control analysis theory.

As seen from Fig. 4, a shift occurs in the enzyme control of the pathway (12 enzymes in the pathway, Fig. 1) from rest, where enzymes far from equilibrium have control, to maximal muscle activity conditions, where enzymes with low V_{max} also exert control. Not included in Fig. 4 is the control of the ATPase, which naturally has the largest impact on the flux (95%–99% of control) over the conditions studied. The general trend is for the increase in flux of the system to reduce the influence of the ATPase (driving force) on the system; but the control by ATPase always remains dominant over the 100-fold range of fluxes analyzed.

At resting flux, with respect to the enzymes within the glycogenolytic and glycolytic pathway, GP and PK are the predominant controls. As the rate of ATP utilization increases, enzymes with lower V_{max} (and thus, less overall flux capacity) such as PFK and PGLM start to share more of the control. At maximal muscle activity, the control coefficients in the pathway have increased relative to the ATPase (summing to 0.05 at their maximal). Thus, they are always much smaller than the control coefficient for the ATPase, and even at high fluxes the system remains ATPase driven. Interestingly, glycogen phosphorylase activity gains importance in the network as flux increases with contractile activity.

Sensitivity analysis of the initial conditions of the metabolite concentrations showed a surprising homogeneity in sensitivity of steady-state concentration values to initial conditions across all energetic states; this sensitivity was overwhelmingly high for all metabolites towards ATP and PCr (detailed results not shown). The sensitivity of the resultant flux toward the metabolites, however, showed differences among the energetic state, as seen in Fig. 5. ATP and ADP remained at similar levels for the

TABLE 5. Values used for 2^{8-4}_{IV} fractional factorial design analysis.

Variable	Low (−) conc. (mM)	High (+) conc. (mM)
P_i	1	40
AMP	1.0E-05	0.05
ADP	0.01	0.5
NADH	5.0E-04	0.01
PCr	3	34.7
GLY	10	100
G6P	0.75	6.7
LAC	1.3	30

different fluxes while P_i, PCr, and glycogen (a fixed value) gradually increase their share in control as fluxes increase. AMP sensitivity was negligible for all states. The sensitivity of intermediates and the systemic flux towards NADH perturbations (and thus redox potential by the conserved moiety) was zero at all flux levels, repeating the observations made by Richard *et al.*[50] regarding redox being completely driven by phosphorylation potential.

Because the previous analysis was performed at a phosphorylase a:b ratio of 40:60, we wanted to investigate the implications of changing the isozyme fractions to the physiological ratio observed under basal conditions. Therefore, the sensitivity analysis was repeated for the case of phosphorylase a:$b = 1\%$:99% for the three ATPase values of 0.6, 6, and 60 mM/min [Fig. 4(b)]. The system is only sensitive to glycogen phosphorylase and phosphofructokinase at resting and moderate exercise conditions; this reflects the greater dependence of the pathway on AMP-dependent reactions to achieve the same flux. Yet, the most surprising result was the system showing the same distributed control pattern over the maximal flux, as seen in Fig. 4(a). The fact that the control pattern is the same for 1% and 40% phosphorylase a reflects a physiologically observed phenomenon—the dephosphorylation back to the b form while maximal muscle activity is still maintained.[9] The differences in the 1% and 40% phosphorylase a analyses at rest and moderate control illustrate the design of the system to shift the sensitivity away from $\sim P$ and towards external effectors (e.g., AMP).

Fractional Factorial Design Analysis

We also performed a two-level fractional factorial design analysis on the metabolite values. By toggling variables in a predetermined pattern of assigned high and low states (as determined by maximal and minimal values found physiologically) and observing the difference in the resultant yield, one can determine the most important factor involved in the yield. For this analysis, the outcome, or yield, of interest is the systemic flux in the pathway as it depends on changes in metabolite concentrations known to occur physiologically (Table 5). A two-level factorial design requires 2^n runs, where n = the number of variables being investigated, to analyze the effects on a system, while a two-level fractional factorial design takes advantage of redundancy in the patterns to simplify analysis. In the analysis performed, 16 runs (2^4) were needed for eight variables instead of 256 (2^8)—the notation 2^{8-4} is used to signify the fractional factorial design used. Readers interested in the details of these calculations are referred to Box *et al.*[6] The definition of a main effect is the size of the difference between the average yield for the runs at the high value minus the average yield for the runs performed at the low value: $\overline{y}_+ - \overline{y}_-$. The analysis used a series of 16 simulations based upon initial conditions of eight variables that vary significantly over the course of muscle activity (P_i, AMP, ADP, PCr, NADH, GLY, G6P, LAC); the metabolite values used are given in Table 5. The values chosen are typical for different levels of muscle activity and were based on the range of values reported from resting to active muscle.[10] ATP was not included among these variables due to its near-constant intracellular concentration.

ADP emerged as the dominant main effect on the flux (10× greater than the next main effect value), with PCr and AMP as secondary main effects (Table 6). The dominant contributor to the largest mixed effect term was the combination of ADP and P_i. This result, of course, is congruent with preexisting knowledge of the $\sim P$ control on the system. It differs, however, from the conventional sensitivity analysis where ADP played a minor role in control in comparison to ATP.

DISCUSSION

Is There a Value in Making All the Reactions Biochemically Reversible in the Equations?

Some of the glycolysis models in the literature have violated the thermodynamic principle of microscopic reversibility by parameter fitting that does not maintain the Haldane relation or by fitting the equilibrium constants of the reaction. We constructed a fully reversible series of equations to represent the glycogenolytic system in skeletal muscle so that an accurate measure of the deviation of the model results from the observed K_{eq} could be made. Cornish-Bowden and Cardenas have delineated how irreversibility versus reversibility of a reaction, even one far from equilibrium, alters the control of a pathway if feedback inhibition is not built into the system.[13] In the model at hand, feedback inhibition through ATP is present at phosphofructokinase, but not at other steps typically considered unidirectional, such as pyruvate kinase. For these reasons, we argue the necessity of includ-

TABLE 6. Design matrix for 2^{8-4}_{IV} fractional factorial design analysis.

Run	P_i	AMP	ADP	NADH	PCr	GLY	G6P	LAC
1	−	−	−	+	+	+	−	+
2	+	−	−	−	−	+	+	+
3	−	+	−	−	+	−	+	+
4	+	+	−	+	−	−	−	+
5	−	−	+	+	−	−	+	+
6	+	−	+	−	+	−	−	+
7	−	+	+	−	−	+	−	+
8	+	+	+	+	+	+	+	+
9	+	+	+	−	−	−	+	−
10	−	+	+	+	+	−	−	−
11	+	−	+	+	−	+	−	−
12	−	−	+	−	+	+	+	−
13	+	+	−	−	+	+	−	−
14	−	+	−	+	−	+	+	−
15	+	−	−	+	+	−	+	−
16	−	−	−	−	−	−	−	−
Main effects	7.64E-07	1.65E-05	1.59E-04	1.72E-06	4.24E-06	5.03E-06	2.78E-06	4.33E-06
17	+	+	+	+	+	−	−	+
18	+	+	+	+	+	−	+	−
19	+	+	+	+	+	+	−	−
20	+	+	+	+	+	+	+	+
Mixed effects	ADP:P_i 5.2e-4	PCr:LAC 3.4e-6	AMP:G6P 1.1e-6	NADH:GLY 1.0e-6				
Largest mixed effect consists of ADP:P_i, AMP:G6P, GLY:NADH, PCr:LAC								

ing the reverse direction in each of our kinetic equations, despite the added complexity and additional parameters needed, and we recommend this practice in general. Such an approach proved useful here because thermodynamics can be employed as a useful tool for validation of the model structure. As the equations are structured, any combination of kinetic values would arrive at the correct K_{eqcombo} as long as the Haldane relation is used. However, only physiologically appropriate kinetic parameter values will result in reasonable fluxes and accurate dynamics. This property was later tested by the ability of the model to simulate steady-state fluxes over a large range of fluxes. A secondary benefit is the prediction of metabolite influences on nonlinear behavior once physiological conditions are imposed. For example, the large control of ADP and P_i and relative unimportance of lactate on the system is highlighted by examining the dynamics of each variable that contributes to the combined K_{eq} of the pathway as the closed system approaches equilibrium (Fig. 2). This is indeed seen in the subsequent fractional factorial design analysis, with ADP main effects and ADP:P_i mixed effects dominating the system (Table 6).

What are the Consequences of the Regulation to Glycogenolytic Flux by Coupling to Other Reactions Within the Cell?

The bulk of glycolytic modeling has been performed in simpler cell types (erythrocyte, yeast). Despite the common emphasis on the minimal glycolysis network *per se* in these models, enormous differences in metabolic regulation among different cell types occurs depending on which additional pathway structures are included. In a detailed red blood cell model by Mulquiney and Kuchel,[39] the 2,3DPG shunt modulating hemoglobin binding is essential to the functionality of oxygen binding. A thorough metabolic control analysis on the model showed primary control of the glycolytic flux occurred via 2,3DPG and nonglycolytic ATPase. In yeast, Teusink *et al.*[61] determined that additional pathways, like the glycerol-3-phosphate dehydrogenase shunt, are necessary to reproduce steady-state data for glycolysis. The common feature of these results suggests a common principle: the regulation of glycolytic flux is controlled differently in different cells because the boundary conditions and connectivity with reactions extrinsic to the main pathway are different.

We asked what effect the boundary conditions and connectivity unique to skeletal muscle—the necessary energetic buffering reactions, large range of metabolite concentrations, and large range of ATPase flux magnitudes—would have on regulation of the flux. The most readily apparent feature of energetic buffering is the damping of transients in ATP due to the capacitance of the phosphate pools (phosphocreatine for creatine kinase and ADP for adenylate kinase). Besides the buffering holding the concentration of ATP constant, the combined action of cellular ATPases and buffer reactions renders changes in the concentration of ADP to the range of tens to hundreds of micromolar, AMP to the range of nanomolar to micromolar, and inorganic phosphate to tens of millimolar. The wide physiological range of these three metabolites then act to increase the glycogenolytic flux as substrate (ADP, P_i) and activators (AMP) in the system.

The ATPase coupling to glycolysis is unique among the models of glycolysis for other cell types. As with yeast and red blood cell, the importance of the ATPase in driving the system emerged with control analysis. However, while the red blood cell model showed control coefficients for the ATPase from 0.67 to 0.886 for the glycolytic fluxes,[39] the skeletal muscle shows larger domination (0.95–0.99) by the energetic demands of the ATPase. As outlined by Hofmeyr[25] and further commented upon by Teusink,[60] a highly efficient metabolic network should be controlled from the demand, not the supply side. This argument also renders meaningless any physiological discussion of rate-limiting steps within a pathway such as glycolysis because such an argument omits the fact that reactions external to the pathway exert >0.95 of the control strength. The historical fallacy of referring to rate-limiting steps in glycolysis without integration with other intracellular processes is a point addressed by Hofmeyr and Cornish-Bowden.[26]

What Aspects of the Network of Reactions are Able to Account for the Ability to Achieve and Sustain a Wide Range of Fluxes?

We attempted to understand the regulation of the pathway at different rates of ATP utilization through sensitivity analysis and fractional factorial design analysis. The sensitivity analysis for three different physiologically relevant fluxes demonstrates a shift in control within the enzymes for glycolysis as fluxes increase towards maximal muscle activity with glycogen phosphorylase becoming the predominant control within the pathway itself under the highest flux. However, under the maximal flux conditions, control is more distributed among pathway enzymes, including near-equilibrium steps often omitted from computational models (phosphoglucomutase, aldolase, enolase). When the phosphorylase ratio is altered to a deactivated basal state, glycogen phosphorylase and phosphofructokinase become the singular source of flux control within the pathway for resting and moderate exercise, highlighting the dependence on AMP at these steps. These interesting features of control within the reactions of glycolysis are minor compared to the control exerted by ATPase.

The results of our factorial design demonstrates that exploring the complete domain of concentration values observed *in vivo* can elicit a different interpretation of primary controllers in an intact system. The two forms of analysis provide different information. The sensitivity analysis allows a straightforward method of altering each variable and observing the consequence on the system when each variable is perturbed in a constant proportion (1%). The available range that a variable can achieve *in vivo*, however, is not proportional to the order of magnitude of its concentration. For example, ADP in basal conditions exists at a relatively low concentration compared to other metabolites in the system (~ 0.01 mM). A sensitivity analysis that perturbs ADP by 1% does not show significant control in the system. However, ADP changes >50-fold over the course of muscle activity. The fractional factorial design is useful in exploring the upper and lower bounds of variable values, as they exist *in vivo*. When we toggle between the basal and fatigue levels of ADP (0.01–0.5 mM), a larger difference in the resulting flux relative to other metabolites becomes obvious. The conventional sensitivity analysis, however, is useful in examining the control exerted by enzyme activities as enzyme activity is constant for the model analyzed here.

The results of the fractional factorial design and the sensitivity analyses indicate the following: (1) The primary function of the phosphorylase isozyme intraconversion is not necessary to achieve maximal fluxes, but rather to shift the distribution of pathway control at low and moderate fluxes. By making the low and moderate fluxes controlled by the AMP-dependent enzymes, a signaling mechanism can easily be elicited due to the connection of the adenylate kinase buffering to the network as described in the prior section of this discussion. (2) The apparently conflicting results of the two forms of analyses actually indicate the common theme of phosphorylation potential control of the system. The network structure of the ATPase with the pathway drives the system and contributes to the ATP, ADP, and P_i concentrations which then, through substrate effects, lead to increase or reduction of the flux. Steady states at the different flux rates are sustainable due to the balanced stoichiometry of the system.

Despite the success of the present model, the physiological reality can be more complex. Conflicting results in the human muscle for the transition from rest to maximal glycolytic fluxes (significant delay in turning on

glycogenolysis[15] versus rapid onset[43]) demonstrate that the details of glycolytic flux dynamics are not fully understood. Although the work presented here focuses on steady-state fluxes, the kinetic model is capable of distinguishing hypotheses of transient mechanisms.

Limitations of the Model

Ideally, the kinetic parameters listed in Table 1 would be obtained from *in vivo* observations under identical conditions and from the same species. Unfortunately, no such data set exists in the literature. This information is needed for a correct analysis of any particular muscle cell type. Despite the complexity and numerous parameters that are imposed on the model, Eq. (1) is itself a simplification from altered binding affinity for bi–bi reactions. This simplification resulted from a lack of information on random binding patterns, especially in the gluconeogenic direction. Thus, the model is limited in the accurate mathematical representation as well as the possible parameter values used. However, the appropriateness of using multiple species to create a consensus is justified by an interspecies similarity in binding constants across mammals.[1,7] Additionally, although interspecies enzyme concentrations vary, the proportionality of enzyme concentrations remains fairly constant.[4,47]

ACKNOWLEDGMENTS

This work was supported by a graduate fellowship to one of the authors (M.J.L.) from the Whitaker Foundation, and by NIH Grant Nos. AR AR45184 awarded to K. Conley and AR AR36281 and AR AR41928 awarded to one of the authors (M.J.K.). Paolo Vicini gave invaluable assistance with the use of the SAAM II software. Zheng Li gave invaluable assistance with the use of the XSIM software tool. Kevin Conley provided insight into the use of fractional factorial sensitivity analysis. Bryant Chase, Kevin Conley, and Greg Crowther patiently read early versions of the paper and made valuable contributions.

APPENDIX: MODEL EQUATIONS

Differential Equations

$$\mathrm{GLY}' = -\mathrm{flux}_{\mathrm{GP}},$$

$$\mathrm{G1P}' = \mathrm{flux}_{\mathrm{GP}} - V_{\mathrm{PGLM}},$$

$$G6P' = V_{\mathrm{PGLM}} - V_{\mathrm{PGI}},$$

$$F6P' = V_{\mathrm{PGI}} - V_{\mathrm{PFK}},$$

$$\mathrm{FBP}' = V_{\mathrm{PFK}} - V_{\mathrm{ALD}},$$

$$\mathrm{DHAP}' = V_{\mathrm{ALD}} + V_{\mathrm{TPI}},$$

$$\mathrm{GAP}' = V_{\mathrm{ALD}} - V_{\mathrm{TPI}} - V_{\mathrm{GAPDH}},$$

$$13\mathrm{BPG}' = V_{\mathrm{GAPDH}} - V_{\mathrm{PGK}},$$

$$3\mathrm{PG}' = V_{\mathrm{PGK}} - V_{\mathrm{PGM}},$$

$$2\mathrm{PG} = V_{\mathrm{PGM}} - V_{\mathrm{ENOL}},$$

$$\mathrm{PEP}' = V_{\mathrm{ENOL}} - V_{\mathrm{PK}},$$

$$\mathrm{PYR}' = V_{\mathrm{PK}} - V_{\mathrm{LDH}},$$

$$\mathrm{LAC}' = V_{\mathrm{LDH}} - \mathrm{output},$$

$$P_i' = -\mathrm{flux}_{\mathrm{GP}} - V_{\mathrm{GAPDH}} + V_{\mathrm{ATPase}},$$

$$\mathrm{ADP}' = V_{\mathrm{PFK}} - V_{\mathrm{PGK}} - V_{\mathrm{PK}} + 2V_{\mathrm{ADK}} + V_{\mathrm{CK}} + V_{\mathrm{ATPase}},$$

$$\mathrm{ATP}' = -V_{\mathrm{PFK}} + V_{\mathrm{PGK}} + V_{\mathrm{PK}} - V_{\mathrm{ADK}} - V_{\mathrm{CK}} - V_{\mathrm{ATPase}},$$

$$\mathrm{AMP}' = -V_{\mathrm{ADK}},$$

$$\mathrm{PCr}' = V_{\mathrm{CK}},$$

$$\mathrm{Cr}' = -V_{\mathrm{CK}},$$

$$\mathrm{NADH} = V_{\mathrm{GAPDH}} - V_{\mathrm{LDH}},$$

$$\mathrm{NAD}' = -V_{\mathrm{GAPDH}} + V_{\mathrm{LDH}}.$$

Glycogen Phosphorylase

The user designates the fraction of isozymes *A* and *B* of glycogen phosphorylase, instead of the inclusion of a function describing phosphorylase kinase activation in the model. Detailed allosteric kinetics of the enzyme available in the literature do not include phosphate as a substrate in the reaction equations, and therefore, are not utilized in our model.[32] As a result, a rapid-equilibrium bi–bi equation is used instead. Isozyme *B* differs from *A* by AMP dependence for catalytic activity, described by an essential cooperative activator term:[56]

$$\mathrm{Glycogen}_n + \Sigma P_i \leftrightarrow \mathrm{Glycogen}_{n-1} + \mathrm{Glucose\text{-}1\text{-}}P$$

$$V_{\mathrm{GPa}}=\frac{V_{\max f}\left(\frac{\mathrm{GLY}\ P_i}{K_{i\mathrm{GLY}f}K_{P_i}}\right)-V_{\max r}\left(\frac{\mathrm{GLY}\ G1P}{K_{\mathrm{GLY}b}\cdot K_{iG1P}}\right)}{\left(1+\frac{\mathrm{GLY}}{K_{i\mathrm{GLY}f}}+\frac{P_i}{K_{iPi}}+\frac{GLY}{K_{i\mathrm{GLY}b}}+\frac{G1P}{K_{iG1P}}+\frac{\mathrm{GLY}\ P_i}{K_{\mathrm{GLY}f}K_{iP_i}}+\frac{GLY\ G1P}{K_{\mathrm{GLY}b}K_{iG1P}}\right)},$$

$$V_{\max r}=\frac{V_{\max f}K_{\mathrm{GLY}b}K_{iG1P}}{K_{i\mathrm{GLY}f}K_{Pi}K_{\mathrm{eqGP}}},$$

$$V_{\mathrm{GPb}}=\frac{V_{\max f}\left(\frac{\mathrm{GLY}\ P_i}{K_{i\mathrm{GLY}f}K_{P_i}}\right)-V_{\max r}\left(\frac{\mathrm{GLY}\ G1P}{K_{i\mathrm{GLY}b}\cdot K_{G1P}}\right)}{\left(1+\frac{GLY}{K_{i\mathrm{GLY}f}}+\frac{P_i}{K_{iP_i}}+\frac{GLY}{K_{i\mathrm{GLY}b}}+\frac{G1P}{K_{iG1P}}+\frac{GLY\ P_i}{K_{i\mathrm{GLY}f}K_{Pi}}+\frac{GLY\ G1P}{K_{i\mathrm{GLY}b}\cdot K_{G1P}}\right)}\frac{\left(\frac{\mathrm{AMP}^{nH}}{K'_{\mathrm{amp}}}\right)}{\left(1+\frac{\mathrm{AMP}^{nH}}{K'_{\mathrm{AMP}}}\right)},$$

$$V_{\max r}=\frac{V_{\max f}\ K_{i\mathrm{GLY}b}\ K_{G1P}}{K_{\mathrm{GLY}f}K_{iP_i}K_{\mathrm{eqGP}}},$$

$$\mathrm{flux}_{\mathrm{GP}}=\mathrm{frac}_a V_{\mathrm{GPa}}+\mathrm{frac}_b V_{\mathrm{GPb}}.$$

Phosphoglucomutase and Phosphoglucoisomerase

Due to the standard reporting of the PGI K_{eq} in the gluconeogenic direction, the Haldane relation defines the $V_{\max f}$ instead of the $V_{\max r}$.

Glucose-1-P↔Glucose-6-P

$$V_{\mathrm{PGLM}}=\frac{\left(V_{\max f}\frac{G1P}{K_{G1P}}\right)-\left(V_{\max r}\frac{G6P}{K_{G6P}}\right)}{1+\frac{G1P}{K_{G1P}}+\frac{G6P}{K_{G6P}}},$$

$$V_{\max r}=\frac{V_{\max f}K_{G6P}}{K_{G1P}K_{\mathrm{eqPGLM}}}.$$

Glucose-6-P↔Fructose-6-P

$$V_{\mathrm{PGI}}=\frac{\left(V_{\max f}\frac{G6P}{K_{G6P}}\right)-\left(V_{\max r}\frac{F6P}{K_{F6P}}\right)}{1+\frac{G6P}{K_{G6P}}+\frac{F6P}{K_{F6P}}},$$

$$V_{\max f}=\frac{V_{\max r}K_{G6P}K_{\mathrm{eqPGI}}}{K_{F6P}}.$$

Phosphofructokinase

We do not include a major PFK inhibitor, citrate, because studies of the effects on skeletal muscle PFK at a physiological range of citrate concentration showed very little inhibition,[46] nor do we include pH effects of PFK within the scope of this paper. Several authors have modeled the skeletal muscle PFK kinetics based on *in vitro* assays, resulting in widely disparate descriptions of the dynamic behavior.[59,65] Due to our requirements that the equation be thermodynamically valid and reversible, we used a reversible two-substrate allosteric equation of the form derived by Popova and Selkov,[48] with allosteric term L defined as described by Nagata *et al.*[40] The L term includes AMP activation and ATP inhibition. The notation K' represents altered binding properties due to the active state of the enzyme.

Fructose-6-P+ΣATP↔Fructose-1,6-P+ΣADP

$$V_{\mathrm{PFK}}=\left(\frac{V_{\max f}\left(\frac{\mathrm{ATP}\ F6P}{K_{\mathrm{ATP}}K_{F6P}}\right)-V_{\max r}\left(\frac{\mathrm{ADP}\ \mathrm{FBP}}{K_{\mathrm{ADP}}K_{\mathrm{FBP}}}\right)}{\Delta}\right)\times\left(\frac{1+\alpha L\left(\frac{\Delta'}{\Delta}\right)^3}{1+L\left(\frac{\Delta'}{\Delta}\right)^4}\right),$$

$$\Delta=\left(1+\frac{F6P}{K_{F6P}}\right)\cdot\left(1+\frac{\mathrm{ATP}}{K_{\mathrm{ATP}}}\right)+\frac{\mathrm{ADP}}{K_{\mathrm{ADP}}}+\frac{\mathrm{FBP}}{K_{\mathrm{FBP}}}\times\left(1+\frac{\mathrm{ADP}}{K_{\mathrm{ADP}}}\right),$$

$$\Delta' = \left(1 + \frac{F6P}{K'_{F6P}}\right) \cdot \left(1 + \frac{\mathrm{ATP}}{K'_{\mathrm{ATP}}}\right) + \frac{\mathrm{ADP}}{K'_{\mathrm{ADP}}} + \frac{\mathrm{FBP}}{K'_{\mathrm{FBP}}} \times \left(1 + \frac{\mathrm{ADP}}{K'_{\mathrm{ADP}}}\right),$$

$$\alpha = \frac{K_{F6P}\, K_{\mathrm{ATP}}}{K'_{F6P}\, K'_{\mathrm{ATP}}},$$

$$L = L_o \left[\left(\frac{1 + \frac{\mathrm{ATP}}{K_{i\mathrm{ATP}}}}{1 + d\frac{\mathrm{ATP}}{K_{i\mathrm{ATP}}}} \right) \cdot \left(\frac{1 + e\frac{\mathrm{AMP}}{K_{a\mathrm{AMP}}}}{1 + \frac{\mathrm{AMP}}{K_{a\mathrm{AMP}}}} \right) \right]^4,$$

$$V_{\max r} = \frac{V_{\max f} K_{\mathrm{ADP}} K_{\mathrm{FBP}}}{K_{\mathrm{ATP}} K_{F6P}}.$$

Aldolase and Triose Phosphate Isomerase

$$\text{Fructose-1,6-P} \leftrightarrow \text{Glyceraldehyde-3-P} + \text{Dihydroxyacetone-P}$$

$$V_{\mathrm{ALD}} = \frac{\left(V_{\max f}\frac{\mathrm{FBP}}{K_{\mathrm{FBP}}}\right) - \left(V_{\max r}\frac{\mathrm{DHAP}\ \mathrm{GAP}}{K_{\mathrm{DHAP}} K_{\mathrm{GAP}}}\right)}{1 + \frac{\mathrm{FBP}}{K_{\mathrm{FBP}}} + \frac{\mathrm{DHAP}}{K_{\mathrm{DHAP}}} + \frac{\mathrm{GAP}}{K_{\mathrm{GAP}}}},$$

$$V_{\max r} = \frac{V_{\max f} K_{\mathrm{DHAP}} K_{\mathrm{GAP}}}{K_{\mathrm{FBP}} K_{\mathrm{eqALD}}}.$$

The forward direction of TPI is defined as producing dihydroxyacetone phosphate.

$$\text{Glyceraldehyde-3-P} \leftrightarrow \text{Dihydroxyacetone-P}$$

$$V_{\mathrm{TPI}} = \frac{\left(V_{\max f}\frac{\mathrm{GAP}}{K_{\mathrm{GAP}}}\right) - \left(V_{\max r}\frac{\mathrm{DHAP}}{K_{\mathrm{DHAP}}}\right)}{1 + \frac{\mathrm{GAP}}{K_{\mathrm{GAP}}} + \frac{\mathrm{DHAP}}{K_{\mathrm{DHAP}}}},$$

$$V_{\max r} = \frac{V_{\max f} K_{\mathrm{DHAP}}}{K_{\mathrm{GAP}} K_{\mathrm{eqTPI}}}.$$

Glyceraldehyde-3-Phosphate Dehydrogenase (GAPDH)

Although various sources have attributed the kinetics to random ter–bi rapid equilibrium,[21,58] Orsi and Cleland produced data to support an ordered mechanism,[42] reducing the complexity of the denominator by limiting possible enzyme complexes.

$$\text{Glyceraldehyde-3-P} + \mathrm{NAD} + \Sigma \mathrm{P_i} \leftrightarrow \text{1,3-bisphosphoglycerate} + \mathrm{NADH}$$

$$V_{\mathrm{GAPDH}} = \frac{\left(V_{\max f}\frac{\mathrm{GAP}\ \mathrm{NAD}\ P_i}{K_{\mathrm{GAP}} K_{\mathrm{NAD}} K_{P_i}}\right) - \left(V_{\max r}\frac{\mathrm{13BPG}\ \mathrm{NADH}}{K_{\mathrm{13BPG}} K_{\mathrm{NADH}}}\right)}{D_{\mathrm{GAPDH}}},$$

$$D_{\mathrm{GAPDH}} = 1 + \frac{\mathrm{GAP}}{K_{\mathrm{GAP}}} + \frac{\mathrm{NAD}}{K_{\mathrm{NAD}}} + \frac{P_i}{K_{Pi}} + \frac{\mathrm{GAP}\ \mathrm{NAD}}{K_{\mathrm{GAP}} K_{\mathrm{NAD}}} + \frac{\mathrm{GAP}\ \mathrm{NAD}\ P_i}{K_{\mathrm{GAP}} K_{\mathrm{NAD}} K_{P_i}} + \frac{13DPG}{K_{\mathrm{13DPG}}} + \frac{NADH}{K_{\mathrm{NADH}}} + \frac{\mathrm{13BPG}\ \mathrm{NADH}}{K_{\mathrm{13BPG}} K_{\mathrm{NADH}}},$$

$$V_{\max r} = \frac{V_{\max f} K_{\mathrm{13BPG}} K_{\mathrm{NADH}}}{K_{\mathrm{GAP}} K_{\mathrm{NAD}} K_{P_i} K_{\mathrm{eqGAPDH}}}.$$

Phosphoglycerate Kinase

Experimental data for the altered dissociation constants of PGK due to the binding of one substrate/product are not available. Therefore, the reaction equation was constructed as a rapid equilibrium ordered bi–bi equation as described in Eq. (1). Like PGI, this reaction is usually reported with the forward direction towards gluconeogenesis; in keeping with this definition, the Haldane relation defines the $V_{\max f}$:

$$\text{1,3-Bisphosphoglycerate} + \Sigma \mathrm{ADP} \leftrightarrow \text{3-Phosphoglycerate} + \Sigma \mathrm{ATP}$$

$$V_{PGK}=\frac{V_{max\,f}\left(\frac{13BPG\ \ ADP}{K_{13BPG}K_{ADP}}\right)-V_{max\,r}\left(\frac{3PG\ \ ATP}{K_{3PG}K_{ATP}}\right)}{1+\frac{13BPG}{K_{13BPG}}+\frac{ADP}{K_{ADP}}+\frac{13BPG\ \ ADP}{K_{13BPG}K_{ADP}}+\frac{3PG}{K_{3PG}}+\frac{ATP}{K_{ATP}}+\frac{3PG\ \ ATP}{K_{3PG}K_{ATP}}},$$

$$V_{max\,f}=\frac{V_{max\,r}K_{13BPG}K_{ADP}K_{eqPGK}}{K_{3PG}K_{ATP}}.$$

Phosphoglyceromutase and Enolase

3-Phosphoglycerate↔2-Phosphoglycerate

$$V_{PGM}=\frac{\left(V_{max\,f}\frac{3PG}{K_{3PG}}\right)-\left(V_{max\,r}\frac{2PG}{K_{2PG}}\right)}{1+\frac{3PG}{K_{3PG}}+\frac{2PG}{K_{2PG}}},$$

$$V_{max\,r}=\frac{V_{max\,f}K_{2PG}}{K_{3PG}K_{eqPGM}}.$$

2-Phosphoglycerate↔Phosphoenolpyruvate

$$V_{ENOL}=\frac{\left(V_{max\,f}\frac{2PG}{K_{2PG}}\right)-\left(V_{max\,r}\frac{PEP}{K_{PEP}}\right)}{1+\frac{2PG}{K_{2PG}}+\frac{PEP}{K_{PEP}}},$$

$$V_{max\,r}=\frac{V_{max\,f}K_{PEP}}{K_{2PG}K_{eqENOL}}.$$

Pyruvate Kinase (PK)

Pyruvate kinase is often considered an allosteric enzyme in glycolysis; however, the muscle isozyme repeatedly shows a lack of cooperativity, and thus has been assigned a Hill coefficient of 1.[26] ATP has been reported to competitively inhibit ADP in the forward direction, however, these data were produced under initial rate conditions. We assume that the steady-state equation with the presence of the product in the denominator appropriately describes the kinetics. The equation for PK is in rapid equilibrium bi–bi form; several sources describe the reaction as random, however, insufficient data are available for the secondary binding constants in the gluconeogenesis direction:

Phosphoenolpyruvate+ΣADP↔Pyruvate+ΣATP

$$V_{PK}=\frac{\left(V_{max\,f}\frac{PEP\ \ ADP}{K_{PEP}K_{ADP}}\right)-\left(V_{max\,r}\frac{PYR\ \ ATP}{K_{PYR}K_{ATP}}\right)}{1+\frac{PEP}{K_{PEP}}+\frac{ADP}{K_{ADP}}+\frac{PEP\ \ ADP}{K_{PEP}K_{ADP}}+\frac{PYR}{K_{PYR}}+\frac{ATP}{K_{ATP}}+\frac{PYR\ \ ATP}{K_{PYR}K_{ATP}}},$$

$$V_{max\,r}=\frac{V_{max\,f}K_{ATP}K_{PYR}}{K_{PEP}K_{ADP}K_{eqPK}}.$$

Lactate Dehydrogenase (LDH)

Pyruvate+NADH↔Lactate+NAD

$$V_{LDH}=\frac{\left(\frac{V_{max\,f}PYR\ \ NADH}{K_{PYR}K_{NADH}}\right)-\left(\frac{V_{max\,r}LAC\ \ NAD}{K_{LAC}K_{NAD}}\right)}{1+\frac{PYR}{K_{PYR}}+\frac{NADH}{K_{NADH}}+\frac{PYR\ \ NADH}{K_{PYR}K_{NADH}}+\frac{LAC}{K_{LAC}}+\frac{NAD}{K_{NAD}}+\frac{LAC\ \ NAD}{K_{LAC}K_{NAD}}},$$

$$V_{\max r} = \frac{V_{\max f} K_{\mathrm{LAC}} K_{\mathrm{NAD}}}{K_{\mathrm{PYR}} K_{\mathrm{NADH}} K_{\mathrm{eqLDH}}}.$$

ATP Reactions: Creatine Kinase, Adenylate Kinase, ATPase

The equation for creatine kinase represents a Cleland (random ordered) bi–bi reaction without dead-end products. The equation and parameters are from Shimerlik and Cleland as used in a published model by Vicini and Kushmerick.[64]

$$\mathrm{Phosphocreatine} + \Sigma\mathrm{ADP} \leftrightarrow \mathrm{Creatine} + \Sigma\mathrm{ATP}$$

$$V_{\mathrm{CK}} = \frac{V_{\max r} \dfrac{\mathrm{ATP}\ \mathrm{Cr}}{K_{i\mathrm{ATP}} K_{\mathrm{Cr}}} - V_{\max f} \dfrac{\mathrm{ADP}\ \mathrm{PCr}}{K_{i\mathrm{ADP}} K_{\mathrm{PCr}}}}{1 + \dfrac{\mathrm{ADP}}{K_{i\mathrm{ADP}}} + \dfrac{\mathrm{PCr}}{K_{i\mathrm{PCr}}} + \dfrac{\mathrm{ADP}\ \mathrm{PCr}}{K_{i\mathrm{ADP}} \cdot K_{\mathrm{PCr}}} + \dfrac{\mathrm{ATP}}{K_{i\mathrm{ATP}}} + \dfrac{\mathrm{ATP}\ \mathrm{Cr}}{K_{i\mathrm{ATP}} K_{\mathrm{Cr}}}},$$

$$V_{\max f} = \frac{V_{\max r} K_{i\mathrm{ATP}} K_{\mathrm{Cr}} K_{\mathrm{eqCK}}}{K_{i\mathrm{ADP}} K_{\mathrm{PCr}}}.$$

$$\Sigma\mathrm{ATP} + \Sigma\mathrm{AMP} \leftrightarrow 2\Sigma\mathrm{ADP}$$

$$V_{\mathrm{ADK}} = \frac{\left(V_{\max f} \dfrac{\mathrm{ATP}\ \mathrm{AMP}}{K_{\mathrm{ATP}} K_{\mathrm{AMP}}}\right) - \left(V_{\max r} \dfrac{\mathrm{ADP}^2}{K_{\mathrm{ADP}}^2}\right)}{1 + \dfrac{\mathrm{ATP}}{K_{\mathrm{ATP}}} + \dfrac{\mathrm{AMP}}{K_{\mathrm{AMP}}} + \dfrac{\mathrm{ATP}\ \mathrm{AMP}}{K_{\mathrm{ATP}} K_{\mathrm{AMP}}} + \dfrac{2\mathrm{ADP}}{K_{\mathrm{ADP}}} + \dfrac{\mathrm{ADP}^2}{K_{\mathrm{ADP}}^2}},$$

$$V_{\max r} = \frac{V_{\max f} K_{\mathrm{ADP}}^2}{K_{\mathrm{ATP}} K_{\mathrm{AMP}} K_{\mathrm{eqADK}}}.$$

ATPase is defined as a simple mass action flux:

$$\Sigma\mathrm{ATP} \rightarrow \Sigma\mathrm{ADP} + \Sigma\mathrm{P}_i,$$

$$V_{\mathrm{ATPase}} = k\,\mathrm{ATP}.$$

NOMENCLATURE

GLY (glycogen)
G1P (glucose 1-phosphate)
G6P (glucose 6-phosphate)
F6P (fructose 6-phosphate)
FBP (fructose 1,6-bisphosphate)
DHAP (1,3-dihydroxyacetone phosphate)
GAP (glyceraldehyde 3-phosphate)
1,3BPG (glycerate 1,3-bisphosphate)
3PG (glycerate 3-phosphate)
2PG (glycerate 2-phosphate)
PEP (phosphoenolpyruvate)
PYR (pyruvate)
LAC (lactate)
P_i (inorganic phosphate)
PCr (phosphocreatine)
Cr (creatine)
GP (glycogen phosphorylase, E.C. 2.4.1.1)
PGLM (phosphoglucomutase E.C. 5.4.2.2)
PGI (phosphoglucose isomerase, E.C. 5.3.1.9)
PFK (6-phosphofructokinase, E.C. 2.7.1.11)
ALD (fructose-bisphosphate aldolase, E.C. 4.1.2.13)
TPI (triose-phosphate isomerase, E.C. 5.3.1.1)
GAPDH (glyceraldehyde-3-phosphate dehydrogenase, E.C. 1.2.1.12)
PGK (phosphoglycerate kinase, E.C. 2.7.2.3)
PGM (phosphoglycerate mutase, E.C. 5.4.2.1)
ENOL (phosphopyruvate hydratase, E.C. 4.2.1.11)
PK (pyruvate kinase, E.C. 2.7.1.40)
LDH (L-lactate dehydrogenase, E.C. 1.1.1.28)
CK (creatine kinase, E.C. 2.7.3.2)
ADK (adenylate kinase, E.C. 2.7.4.3)
ATPase (myosin ATPase, E.C. 3.6.4.1)

REFERENCES

[1] Achs, M. J., and D. Garfinkel. Metabolism of the acutely ischemic dog heart. I. Construction of a computer model. *Am. J. Physiol.* 236:R21–R30, 1979.
[2] Arnold, H., and D. Pette. Binding of glycolytic enzymes to structure proteins of the muscle. *Eur. J. Biochem.* 6:163–171, 1968.
[3] Bakker, B. M., P. A. M. Michels, F. R. Opperdoes, and H. V. Westerhoff. Glycolysis in bloodstream form Trypanosoma brucei can be understood in terms of the kinetics of the glycolytic enzymes. *J. Biol. Chem.* 272:3207–3215, 1997.
[4] Bass, A., D. Brdiczka, P. Eyer, S. Hofer, and D. Pette. Metabolic differentiation of distinct muscle types at the level of enzymatic organization. *Eur. J. Biochem.* 10:198–206, 1969.
[5] Bennett, N. G., and H. Gutfreund. The kinetics of the interconversion of intermediates of the reaction of pig muscle lactate dehydrogenase with oxidized nicotinamide–adenine dinucleotide and lactate. *Biochem. J.* 135:81–85, 1973.
[6] Box, G. E. P., W. G. Hunter, and J. S. Hunter. Statistics for Experimenters. An Introduction to Design, Data Analysis and Model Building. New York: Wiley, 1978, p. 653.
[7] Cardenas, J. M., E. G. Blachly, P. L. Ceccotti, and R. D. Dyson. Properties of chicken skeletal muscle pyruvate kinase and a proposal for its evolutionary relationship to the other avian and mammalian isozymes. *Biochemistry* 14:2247–2252, 1975.
[8] Cheetham, M. E., L. H. Boobis, S. Brooks, and C. Williams. Human muscle metabolism during sprint running. *J. Appl. Physiol.* 61:54–60, 1986.
[9] Conlee, R. K., J. A. McLane, M. J. Rennie, W. W. Winder, and J. O. Holloszy. Reversal of phosphorylase activation in muscle despite continued contractile activity. *Am. J. Physiol.* 237:R291–R296, 1979.
[10] Conley, K. E., M. L. Blei, T. L. Richards, M. J. Kushmerick,

and S. A. Jubrias. Activation of glycolysis in human muscle *in vivo*. *Am. J. Physiol.* 273:C306–C315, 1997.
[11] Conley, K. E., M. J. Kushmerick, and S. A. Jubrias. Glycolysis is independent of oxygenation state in stimulated human skeletal muscle *in vivo*. *J. Physiol. (London)* 511:935–945, 1998.
[12] Connett, R., and K. Sahlin. Control of glycolysis and glycogen metabolism. In: Handbook of Physiology, edited by L. Rowell and J. Shepherd. New York: Oxford University Press, 1996, Sec. 12, pp. 870–911.
[13] Cornish-Bowden, A., and M. L. Cardenas. Irreversible reactions in metabolic simulations: How reversible is irreversible? In: Animating the Cellular Map, edited by J.-H. S. Hofmeyr, J. H. Rowher, and J. L. Snoep. Stellenbosch: Stellenbosch University Press, 2000, pp. 65–71.
[14] Crerar, M. M., O. Karlsson, R. J. Fletterick, and P. K. Hwang. Chimeric muscle and brain glycogen phosphorylases define protein domains governing isozyme-specific responses to allosteric activation. *J. Biol. Chem.* 270:13748–13756, 1995.
[15] Crowther, G. J., M. F. Carey, W. F. Kemper, and K. E. Conley. Control of glycolysis in contracting skeletal muscle. I. Turning it on. *Am. J. Physiol.* 282:E67–E73, 2002.
[16] Dabrowska, A., I. Kamrowska, and T. Baranowski. Purification, crystallization, and properties of triosephosphate isomerase from human skeletal muscle. *Acta Biochim. Pol.* 25:247–256, 1978.
[17] De Weer, P., and A. G. Lowe. Myokinase equilibrium. An enzymatic method for the determination of stability constants of magnesium complexes with adenosine triphosphate, adenosine diphosphate, and adenosine monophosphate in media of high ionic strength. *J. Biol. Chem.* 248:2829–2835, 1973.
[18] Dyson, R. D., J. M. Cardenas, and R. J. Barsotti. The reversibility of skeletal muscle pyruvate kinase and an assessment of its capacity to support glyconeogenesis. *J. Biol. Chem.* 250:3316–3321, 1975.
[19] Engers, H. D., W. A. Bridger, and N. B. Madsen. Kinetic mechanism of phosphorylase *b*. Rates of initial velocities and of isotope exchange at equilibrium. *J. Biol. Chem.* 244:5936–5942, 1969.
[20] Fifis, T., and R. K. Scopes. Purification of 3-phosphoglycerate kinase from diverse sources by affinity elution chromatography. *Biochem. J.* 175:311–319, 1978.
[21] Furfine, C. S., and S. F. Velick. The acyl-enzyme intermediate and the kinetic mechanism of the glyceraldehyde 3-phosphate dehydrogenase reaction. *J. Biol. Chem.* 240:844–855, 1965.
[22] Garfinkel, D., R. A. Frenkel, and L. Garfinkel. Simulation of the detailed regulation of glycolysis in a heart supernatant preparation. *Comput. Biomed. Res.* 2:68–91, 1968.
[23] Gold, A. M., R. M. Johnson, and J. K. Tseng. Kinetic mechanism of rabbit muscle glycogen phosphorylase *a*. *J. Biol. Chem.* 245:2564–2572, 1970.
[24] Harris, R. C., E. Hultman, and L. O. Nordesjo. Glycogen, glycolytic intermediates, and high-energy phosphates determined in biopsy samples of musculus quadriceps femoris of man at rest. Methods and variance of values. *Scand. J. Clin. Lab. Invest.* 33:109–120, 1974.
[25] Hofmeyr, J. H. Metabolic regulation: A control analytic perspective. *J. Bioenerg. Biomembr.* 27:479–490, 1995.
[26] Hofmeyr, J. S., and A. Cornish-Bowden. Regulating the cellular economy of supply and demand. *FEBS Lett.* 476:47–51, 2000.
[27] Imamura, K., and T. Tanaka. Pyruvate kinase isozymes from rat. *Methods Enzymol.* 90:150–165, 1982.
[28] Johnson, M. J. Enzyme equilibria and thermodynamics. In: The Enzymes, 4, edited by H. L. P. D. Boyer and K. Myrbäck. New York: Academic, 1959, pp. 407–441.
[29] Joshi, A., and B. O. Palsson. Metabolic dynamics in the human red cell. Part III. Metabolic reaction rates. *J. Theor. Biol.* 142:41–68, 1990.
[30] Joshi, J. G., and P. Handler. Phosphoglucomutase. I. Purification and properties of phosphoglucomutase from Escherichia coli. *J. Biol. Chem.* 239:2741, 1964.
[31] Kahana, S. F., O. H. Lowry, D. W. Schulz, J. V. Passoneau, and E. J. Crawford. The kinetics of phosphoglucoisomerase. *J. Biol. Chem.* 235:2178–2184, 1960.
[32] Klinov, S. V., and B. I. Kurganov. Kinetic mechanism of activation of muscle glycogen phosphorylase *b* by adenosine 5′-monophosphate. *Arch. Biochem. Biophys.* 312:14–21, 1994.
[33] Krietsch, W. K., and T. Bucher. 3-phosphoglycerate kinase from rabbit sceletal muscle and yeast. *Eur. J. Biochem.* 17:568–580, 1970.
[34] Krietsch, W. K., P. G. Pentchev, H. Klingenburg, T. Hofstatter, and T. Bucher. The isolation and crystallization of yeast and rabbit liver triose phosphate isomerase and a comparative characterization with the rabbit muscle enzyme. *Eur. J. Biochem.* 14:289–300, 1970.
[35] Mahler, H. R., and E. H. Cordes. Biological Chemistry. New York: Harper and Row, 1971, p. 1009.
[36] Merry, S., and H. G. Britton. The mechanism of rabbit muscle phosphofructokinase at pH8. *Biochem. J.* 226:13–28, 1985.
[37] Minakami, S., and H. Yoshikawa. Studies on erythrocyte glycolysis. II. Free energy changes and rate limitings steps in erythrocyte glycolysis. *J. Biochem. (Tokyo)* 59:139–144, 1966.
[38] Molnar, M., and M. Vas. Mg^{2+} affects the binding of ADP but not ATP to 3-phosphoglycerate kinase. Correlation between equilibrium dialysis binding and enzyme kinetic data. *Biochem. J.* 293:595–599, 1993.
[39] Mulquiney, P. J., and P. W. Kuchel. Model of 2,3-bisphosphoglycerate metabolism in the human erythrocyte based on detailed enzyme kinetic equations: Equations and parameter refinement. *Biochem. J.* 342:581–596, 1999.
[40] Nagata, K., K. Suzuki, and K. Imahori. Analysis of the allosteric properties of rabbit muscle phosphofructokinase by means of affinity labeling with a reactive ATP analog. *J. Biochem. (Tokyo)* 86:1179–1189, 1979.
[41] Nakae, Y., and P. J. Stoward. Kinetic parameters of lactate dehydrogenase in liver and gastrocnemius determined by three quantitative histochemical methods. *J. Histochem. Cytochem.* 45:1427–1431, 1997.
[42] Orsi, B. A., and W. W. Cleland. Inhibition and kinetic mechanism of rabbit muscle glyceraldehyde-3-phosphate dehydrogenase. *Biochemistry* 11:102–109, 1972.
[43] Parolin, M. L., A. Chesley, M. P. Matsos, L. L. Spriet, N. L. Jones, and G. J. Heigenhauser. Regulation of skeletal muscle glycogen phosphorylase and PDH during maximal intermittent exercise. *Am. J. Physiol.* 277:E890–E900, 1999.
[44] Parra, J., J. A. Cadefau, G. Rodas, N. Amigo, and R. Cusso. The distribution of rest periods affects performance and adaptations of energy metabolism induced by high-intensity training in human muscle. *Acta Physiol. Scand.* 169:157–165, 2000.
[45] Penhoet, E. E., M. Kochman, and W. J. Rutter. Isolation of fructose diphosphate aldolases A, B, and C. *Biochemistry* 8:4391–4395, 1969.
[46] Peters, S. J., and L. L. Spriet. Skeletal muscle phosphofruc-

tokinase activity examined under physiological conditions *in vitro*. *J. Appl. Physiol.* 78:1853–1858, 1995.
[47] Pette, D., and H. W. Hofer. The constant proportion enzyme group concept in the selection of reference enzymes in metabolism. *Ciba Found Symp.* 73:231–244, 1979.
[48] Popova, S. V., and E. E. Sel'kov. Description of the kinetics of the two substrate reactions $S1+S2$ goes to and comes from $S3+S4$ by a generalized Monod, Wyman, Changeux model. *Mol. Biol. (Moscow)* 13:129–139, 1979.
[49] Puigjaner, J., B. Rais, M. Burgos, B. Comin, J. Ovadi, and M. Cascante. Comparison of control analysis data using different approaches: Modeling and experiments with muscle extract. *FEBS Lett.* 418:47–52, 1997.
[50] Richard, P., B. Teusink, M. B. Hemker, K. Van Dam, and H. V. Westerhoff. Sustained oscillations in free-energy state and hexose phosphates in yeast. *Yeast* 12:731–740, 1996.
[51] Rider, C. C., and C. B. Taylor. Enolase isoenzymes in rat tissues. Electrophoretic, chromatographic, immunological, and kinetic properties. *Biochim. Biophys. Acta* 365:285–300, 1974.
[52] Rose, Z. B., and S. Dube. Phosphoglycerate mutase. Kinetics and effects of salts on the mutase and bisphosphoglycerate phosphatase activities of the enzyme from chicken breast muscle. *J. Biol. Chem.* 253:8583–8592, 1978.
[53] Sahlin, K. NADH in human skeletal muscle during short-term intense exercise. *Pflugers Arch.* 403:193–196, 1985.
[54] Schimerlik, M. I., and W. W. Cleland. Inhibition of creatine kinase by chromium nucleotides. *J. Biol. Chem.* 248:8418–8123, 1973.
[55] Scopes, R. K. Studies with a reconstituted muscle glycolytic system. The rate and extent of creatine phosphorylation by anaerobic glycolysis. *Biochem. J.* 134:197–208, 1973.
[56] Segel, I. H. Enzyme Kinetics: Behavior and Analysis of Rapid Equilibrium and Steady-State Enzyme Systems. New York: Wiley, 1975, p. 957.
[57] Sempere, S., A. Cortes, and J. Bozal. Kinetic mechanism of guinea-pig skeletal muscle lactate dehydrogenase (M4) with oxaloacetate NADH and pyruvate NADH as substrates. *Int. J. Biochem.* 13:727–731, 1981.
[58] Smith, C. M., and S. F. Velick. The glyceraldehyde 3-phosphate dehydrogenases of liver and muscle. Cooperative interactions and conditions for functional reversibility. *J. Biol. Chem.* 247:273–284, 1972.
[59] Smolen, P. A model for glycolytic oscillations based on skeletal muscle phosphofructokinase kinetics. *J. Theor. Biol.* 174:137–148, 1995.
[60] Teusink, B. Exposing a complex metabolic system: Glycolysis in Saccharomyces cerevisiae. In: Department of Biology, BioCentrum Amsterdam, Amsterdam, The Netherlands: Universiteit van Amsterdam, 1999, p. 231.
[61] Teusink, B., J. Passarge, C. A. Reijenga, E. Esgalhado, C. C. van der Weijden, M. Schepper, M. C. Walsh, B. M. Bakker, K. van Dam, H. V. Westerhoff, and J. L. Snoep. Can yeast glycolysis be understood in terms of *in vitro* kinetics of the constituent enzymes? Testing biochemistry. *Eur. J. Biochem.* 267:5313–5329, 2000.
[62] Thuma, E., R. H. Schirmer, and I. Schirmer. Preparation and characterization of a crystalline human ATP:AMP phosphotransferase. *Biochim. Biophys. Acta* 268:81–91, 1972.
[63] Velick, S. F., and C. Furfine. Glyceraldehyde 3-phosphate dehydrogenase. In: The Enzymes, 7, edited by P. D. Boyer, H. Lardy, and K. Myrbäck. New York: Academic, 1963, Vol. 7, Chap. 12.
[64] Vicini, P., and M. J. Kushmerick. Cellular energetics analysis by a mathematical model of energy balance: Estimation of parameters in human skeletal muscle. *Am. J. Physiol.* 279:C213–C224, 2000.
[65] Waser, M. R., L. Garfinkel, M. C. Kohn, and D. Garfinkel. Computer modeling of muscle phosphofructokinase kinetics. *J. Theor. Biol.* 103:295–312, 1983.
[66] Zewe, V., and H. J. Fromm. Kinetic studies of rabbit muscle lactate dehydrogenase. *J. Biol. Chem.* 237:1668—1675, 1962.